Robustness Analysis of Huygens Atmospheric Entry Flight under Uncertain Initial Conditions

Johannes Robens*
German Aerospace Center (DLR), 82234 Wessling, Germany

Felix Biertümpfel† and Harald Pfifer‡
Technische Universität Dresden, 01062 Dresden, Germany

ESA's Huygens probe had only one attempt to successfully enter Titan's atmosphere. Due to large uncertainties, it was crucial to ensure the mission's robustness during the development phase. Common methods like Monte-Carlo simulations are computationally expensive and provide only a lower bound for worst case values. Therefore, this paper presents a robustness analysis method that determines the upper bound to complement Monte-Carlo simulation results and to increase the confidence in the mission's robustness. The developed method is based on linear time-varying systems and quadratic constraints to describe deviations from the nominal trajectory resulting from a set of uncertain initial conditions.

I. Introduction

In January 2005 as part of NASA/ESA's Cassini-Huygens mission, the Huygens probe landed on Titan, Saturn's largest moon, to conduct scientific measurements in its atmosphere and on its surface [1]. The lander was separated from the orbiter Cassini three weeks prior to the entry flight without having an active control system to stabilize and maneuver the vehicle to its target location. As a result, Huygens' atmospheric entry flight was subject to large uncertainties [2, 3]. Missions such as Huygens are expensive and take a lot of time due to its interplanetary voyage of several years. Therefore, it is crucial to analyze the robustness of the system with respect to expected uncertainties extensively during the development phase to ensure a successful mission.

The robustness analysis of a nonlinear system analyzes the deviation from its nominal trajectory under uncertainties in order to validate compliance with mission requirements. There are many different methods to analyze the robustness of a system, e.g. stochastic methods and worst-case optimizations. The most common method is Monte-Carlo simulations that solve the dynamics for numerous uncertainty combinations. A key advantage of Monte-Carlo simulations is that they simulate the full nonlinear system, thus, they do not necessarily make simplifications and every state and output can be analyzed. However, this fact also renders Monte-Carlo simulations computationally expensive and time consuming, as a large number of simulations is usually required for statistical significance. Additionally, they only provide a lower bound for the requirements, since the actual worst case can only be theoretically found by an infinite amount of simulations. In summary, this slows down the overall development process especially if many design iterations are required. The analysis method developed in this paper addresses these shortcomings by providing worst-case bounds in a fraction of time. The approach linearizes the nonlinear system along its nominal trajectory and re-includes the nonlinear terms by bounds. Therefore, it complements Monte-Carlo simulations by accelerating the development process of the system and providing the upper bound to constrain the worst case from both sides.

There exist already many similar robustness analysis methods [4–8] that, however, are usually based on different assumptions or focus on other objectives. For instance, the paper [4] analyzes discrete-time, uncertain linear time-varying systems (LTV) under unknown initial conditions over a short time period by solving a linear matrix inequality (LMI). The references [5] and [6] consider LTV systems along uncertain trajectories. The former focuses on performance measures at the end of the trajectory due to uncertain parameters and external disturbances, whereas the latter determines a bound for the entire finite time horizon. The publications [7] and [8] concentrate on linear parameter varying systems. In contrast, this paper develops a robustness analysis method that analyzes an autonomous uncertain LTV system under unknown initial conditions over a long time period. Therefore, the robustness condition is solved by integrating a Riccati differential equation backwards in time.

*Research Associate, Institute of Robotics and Mechatronics, johannes.robens@dlr.de
†Research Associate, Chair of Flight Mechanics and Control, AIAA Young Professional, felix.biertuempfel@tu-dresden.de
‡Professor, Chair of Flight Mechanics and Control, harald.pfifer@tu-dresden.de

Section II describes the necessary theoretical preliminaries, e.g. linear time-varying systems or quadratic constraint interconnection, and preparatory steps, e.g. calculating a linear model or bounding the nonlinearities, which are necessary to develop and perform the linear robustness analysis. Thereafter, Section III derives the theorem that allows for determining upper bounds for the system's states and outputs and shortly describes how to solve the theorem. In Section IV, Huygens' atmospheric entry flight is introduced by outlining the relevant properties of Titan and Huygens as well as the assumptions made to derive the nonlinear equations of motion. Subsequently, the linear robustness analysis results of Huygens' entry flight, which are divided in two parts, are discussed in Section V. First, the theorem is solved for the nominal linear model. Thereafter, the full theorem is solved by considering quadratic constraints as well.

II. Background on Uncertain Linear Time-Varying Systems

A. Autonomous Nonlinear System and its Nominal Trajectory

An autonomous nonlinear system can be described by

$$\begin{aligned} \dot{\tilde{x}} &= f(\tilde{x}, p) \\ \tilde{y} &= \tilde{x}. \end{aligned} \tag{1}$$

The differential function f depends on the system states $\tilde{x}(t) \in \mathbb{R}^{n_x}$ and some parameters p and defines the time derivatives $\dot{\tilde{x}}(t)$. In this paper, the states are taken as outputs, i.e. $\tilde{y}(t) = \tilde{x}(t)$. To simplify the notation, the time dependency of the state and output vectors is omitted. The more general case with a nonlinear algebraic function as outputs is described in [9]. Furthermore, nominal initial conditions result in the nominal trajectory of System (1), which is denoted by n, e.g. $\tilde{x}_n$ and $\tilde{y}_n$.

B. Linear Time-Varying System with Uncertain Initial States

A linear time-varying (LTV) system with uncertain initial conditions is defined by

$$\begin{aligned} \dot{x} &= A(t)x + B(t)u \\ y &= C(t)x + D(t)u \end{aligned} \tag{2}$$

$$x(0) = \Gamma\xi. \tag{3}$$

Here, $x(t) \in \mathbb{R}^{n_x}$, $y(t) \in \mathbb{R}^{n_y}$, and $u(t) \in \mathbb{R}^{n_u}$ are the state, output, and input vectors, whereas A, B, C, and D represent matrix valued functions of time as the system, input, output, and feed-through matrices of appropriate dimensions, e.g. $A(t) \in \mathbb{R}^{n_x \times n_x}$. Furthermore, the uncertain initial states $x(0)$ in Eq. (3) follow the proposed method in [4]. The vector $\xi \in \mathbb{R}^a$ with $a \leq n_x$ contains the uncertain initial states and each component ξ_i with $i \in (1, \ldots, a)$ is normalized to the interval $[-1, 1]$. In addition, each uncertain state is considered independently, i.e. it fulfills the constraint $|\xi_i| \leq 1$. Thus, the matrix Γ defines the shape of the uncertainty set as a cuboid.

C. Linearization along Trajectory

The proposed robustness analysis investigates the deviation from the nominal trajectory based on an LTV model defined on the finite time interval $[0, T]$. Therefore, the nonlinear system of Huygens' entry flight, which can be expressed by Eq. (1), is linearized along its nominal trajectory. The resulting dynamics of the trajectory deviation can be described by

$$\begin{aligned} \dot{x} &= f(x + \tilde{x}_n) - f(\tilde{x}_n) = A(t)x + \varepsilon_f \\ y &= x + \tilde{x}_n - \tilde{x}_n = x, \end{aligned} \tag{4}$$

using the state and output deviations $x = \tilde{x} - \tilde{x}_n$ and $y = \tilde{y} - \tilde{y}_n$. Here, $A(t)x$ is the LTV model as in Eq. (2), whereas $\varepsilon_f(t) \in \mathbb{R}^{n_x}$ represents higher order terms. The time dependency of ε_f is also omitted in this paper. The linear model should only include slow instead of high frequency dynamics, e.g. high frequency oscillatory modes, which result from linearizing at untrimmed conditions. Therefore, oscillating states on the nominal trajectory are replaced by trimmed

conditions resulting in $\tilde{x}_t$ and the LTV model is then calculated by $A(t) = \partial f/\partial \tilde{x}|_{\tilde{x}_t}$. Thereafter, the higher order terms can be determined by

$$\varepsilon_f = f(x + \tilde{x}_n) - f(\tilde{x}_n) - A(t)x, \tag{5}$$

showing that ε_f is a function of the states x and time t. Finally, a strictly time-dependent matrix function A is obtained by determining A on a sufficiently high grid on the relevant time interval $[0, T]$ and interpolating values in between with a piecewise cubic Hermite interpolation, e.g. the modified Akima interpolation [10].

D. Quadratic Constraints

The system (4) can be written in a linear fractional representation (LFR) as shown in Fig. 1a. Here, G represents the nominal time variant dynamics and Δ the nonlinear function (5) as the perturbation of the nominal dynamics. In order to include the nonlinearities in the robustness analysis, the system needs to be transformed into the quadratic constraint (QC) framework [11–13] resulting in the interconnection depicted in Fig. 1b. Thus, the Δ block is excluded from the interconnection, the higher order terms ε_f are considered as inputs, and the Δ block's input and output signals are combined to a new output z. The QC interconnection is mathematically described by

$$\begin{aligned} \dot{x} &= A(t)x + B\varepsilon_f \\ y &= x \\ z &= Cx + D\varepsilon_f, \end{aligned} \tag{6}$$

with B being the identity matrix or the appropriate columns, if not all components of ε_f are used. The matrices C and D concatenate x and ε_f to the vector z. Additionally, a time dependent quadratic constraint on the output z over the relevant time interval $[0, T]$ is defined by

$$z^T M(t) z \geq 0, \quad M = M^T \tag{7}$$

to bound the input/output behavior of the nonlinear function (5). Each higher order term component $\varepsilon_{f,k}$ with $k \in (1, \ldots, n_x)$ is bounded individually by $z_k = \begin{bmatrix} x^T & \varepsilon_{f,k} \end{bmatrix}^T$ and

$$M_k = \begin{bmatrix} M_{11,k} & M_{12,k} \\ M_{12,k}^T & -1 \end{bmatrix}, \quad M_{11,k} = M_{11,k}^T. \tag{8}$$

The individual constraints are also defined as local, thus, they only bound the ε_f components correctly in a certain region around the nominal trajectory. The values of the matrix $M_{11,k}$ and the vector $M_{12,k}$ are determined by the following linear optimization:

$$\begin{aligned} \min_{M_{11,k}, M_{12,k}} \quad & \sum_{j=1}^{b} z_j^T \begin{bmatrix} M_{11,k} & M_{12,k} \\ M_{12,k}^T & -1 \end{bmatrix} z_j \\ \text{s.t.} \quad & z_j^T \begin{bmatrix} M_{11,k} & M_{12,k} \\ M_{12,k}^T & -1 \end{bmatrix} z_j \geq 0 \quad \forall j \in \{1, \ldots, b\} \\ & M_{11,k} = M_{11,k}^T. \end{aligned} \tag{9}$$

Firstly, the considered region around the nominal trajectory is approximated by b evaluation points with each providing a z_j vector. Furthermore, the optimization problem is subject to the desired quadratic constraint being imposed on every evaluated point and $M_{11,k}$ being symmetric. Lastly, the sum of the desired quadratic constraint applied to the evaluated points is minimized to obtain the least conservative quadratic constraint M_k. Thereafter, the vector z and the matrix M in Eq. (7) are obtained by concatenating the individual vectors z_k to one vector z and the matrices M_k to a block diagonal matrix $M = diag(M_1, \ldots, M_{n_x})$ with $k \in (1, \ldots, n_x)$. To reduce conservatism, the quadratic constraint (7) is time dependent. Similarly to Subsection II.C, this is achieved by calculating the quadratic constraints on a grid of the relevant time interval $[0, T]$ and determining values in between with a modified Akima interpolation. To conclude, System (6) and the quadratic constraint (7) form an appropriate LTV model for the robustness analysis.

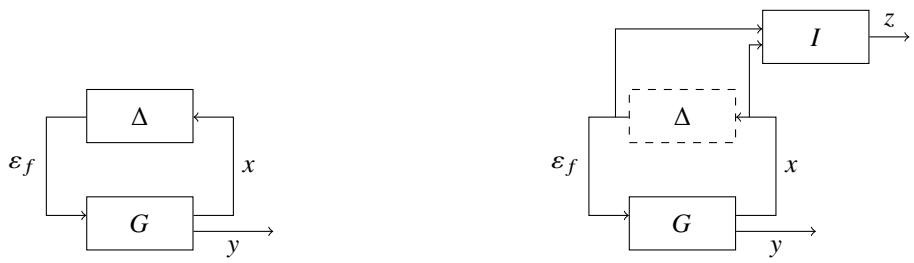

Fig. 1 (a) linear fractional representation, (b) QC interconnection

III. Robustness Analysis for QC Interconnections

A. Theorem Derivation

The upper bound γ on worst-case values of the uncertain LTV system's outputs y in (4) at time point T is defined over the set of uncertain initial conditions ξ. This bound is expressed using the Euclidean norm as

$$\sup_{\xi_i \leq 1 \forall i \in (1,\ldots,a)} \|y(T)\| \leq \gamma. \tag{10}$$

The following theorem provides sufficient conditions based on dissipation arguments to calculate the upper bound.

Theorem 1. *Let Eq.* (6) *define the LTV system,* $x(0)$ *be the uncertain initial state bounded by Eq.* (3)*, and* M *be the block diagonal matrix* $M = diag\big(M_1, \ldots, M_{n_x}\big)$ *from Eq.* (7)*. Assume there exists scalars* $\gamma \geq 0$*,* $v_i \geq 0$ *for* $i \in (1, ..., a)$ *with* $V_0 = diag(v_1, \ldots, v_a)$*, and* $\lambda_k \geq 0$ *for* $k \in (1, \ldots, n_x)$ *with* $\Lambda = diag\big(\lambda_1 I_{n_x+1}, \ldots, \lambda_{n_x} I_{n_x+1}\big)$*, together with a continuous function* $P : \mathbb{R} \rightarrow \mathbb{R}^{n_x \times n_x}$*. If the equations*

$$\dot{P} = -PA - A^T P - C^T \Lambda M C + \Big(PB + C^T \Lambda M D\Big)\Big(D^T \Lambda M D\Big)^{-1}\Big(B^T P + D^T \Lambda M C\Big) \quad \forall t \in [0, T] \tag{11}$$

$$I - P(T) = 0 \tag{12}$$

$$\begin{bmatrix} \Gamma^T P(0) \Gamma - V_0 & 0 \\ 0 & v_1 + \ldots + v_a - \gamma^2 \end{bmatrix} \leq 0 \tag{13}$$

are satisfied, then, the following inequality holds

$$\sup_{\xi_i \leq 1 \forall i \in (1,\ldots,a)} \|y(T)\| \leq \gamma. \tag{14}$$

Proof. The proof is based on the positive definite storage function $V(x, t) = x^T P(t) x$. First, we perturb Eq. (11) with an infinitesimal small positive scalar ϵ resulting in

$$\dot{P} + PA + A^T P + C^T \Lambda M C - \Big(PB + C^T \Lambda M D\Big)\Big(D^T \Lambda M D\Big)^{-1}\Big(B^T P + D^T \Lambda M C\Big) - I_{n_x} \epsilon \leq 0. \tag{15}$$

After applying the Schur complement [14] on Eq. (15) and left and right multiplying the resulting matrix inequality with $\begin{pmatrix} x^T & \varepsilon_f^T \end{pmatrix}$ and $\begin{pmatrix} x^T & \varepsilon_f^T \end{pmatrix}^T$, respectively, we obtain

$$\begin{pmatrix} x \\ \varepsilon_f \end{pmatrix}^T \begin{bmatrix} A^T P + \dot{P} + PA - I_{n_x} \epsilon & PB \\ B^T P & 0 \end{bmatrix} \begin{pmatrix} x \\ \varepsilon_f \end{pmatrix} + \begin{pmatrix} x \\ \varepsilon_f \end{pmatrix}^T \begin{pmatrix} C & D \end{pmatrix}^T \Lambda M \begin{pmatrix} C & D \end{pmatrix} \begin{pmatrix} x \\ \varepsilon_f \end{pmatrix} \leq 0. \tag{16}$$

Here, the right term is equal to Eq. (7), i.e. always ≥ 0, and can thus be removed from the above inequality. By further rewriting the remaining left side of Eq. (16), we get

$$\begin{pmatrix} x \\ \varepsilon_f \end{pmatrix}^T \begin{bmatrix} A^T P + \dot{P} + PA & PB \\ B^T P & 0 \end{bmatrix} \begin{pmatrix} x \\ \varepsilon_f \end{pmatrix} - \epsilon x^T x \leq 0. \tag{17}$$

The left term represents $\dot{V}$, whereas $\epsilon x^T x \approx 0$. Therefore, it results $\dot{V} \leq 0$. Next, Eqs. (12) and (13) together with $\dot{V} \leq 0$ are used to establish $\|y(T)\| \leq \gamma$. We first left and right multiply Eq. (12) with $x^T(T)$ and $x(T)$, respectively, and Eq. (13) with $\left(\xi^T, 1\right)$ and $\left(\xi^T, 1\right)^T$, respectively. After adding both equations, we obtain

$$x^T(0)P(0)x(0) - \xi^T V_0 \xi + x^T(T)x(T) - x^T(T)P(T)x(T) + v_1 + \ldots + v_a - \gamma^2 \leq 0. \tag{18}$$

Since $\dot{V} \leq 0$, we can exclude $V(0) - V(T) = x^T(0)P(0)x(0) - x^T(T)P(T)x(T) \geq 0$ from the above inequality. Furthermore, we replace $\xi^T V_0 \xi$ with the equivalent expression $v_1\xi_1^2 + \ldots + v_a\xi_a^2$ and rearrange the terms to get

$$v_1\left(1 - \xi_1^2\right) + \ldots + v_a\left(1 - \xi_a^2\right) \leq \gamma^2 - x^T(T)x(T). \tag{19}$$

Due to $v_i \geq 0$ and $|\xi_i| \leq 1$, the left hand side is nonnegative. Hence, the right hand side must also be nonnegative and can, therefore, be written as

$$x^T(T)x(T) \leq \gamma^2. \tag{20}$$

As shown in Eq. (6), we can replace x by y in the above equation, which results in the main statement (14) and, thus, concludes the proof. □

B. Solution Approach

In order to perform the robustness analysis, Theorem 1 needs to be transformed into a computational tractable problem to solve for the least conservative worst-case upper bound γ. Since the parameters v_i, and λ_k can be chosen freely, the goal is to optimize γ over these parameters. The optimization starts by using $P(T)$ from Eq. (12) as initial condition for the Riccati differential equation (RDE) (11). The RDE is then integrated backwards in time from T to 0 [15], which yields $P(0)$. At each integration step, the λ_k values are determined analytically by minimizing the contribution of the quadratic constraints. Finally, the linear matrix inequality (LMI) (13) is solved for γ^2 by using the Yalmip toolbox [16] with Mosek* as a solver. Detailed information about the solution approach are given in [9].

IV. Problem Formulation

The developed robustness analysis is applied to the entry flight of NASA/ESA's Cassini-Huygens mission from 2005. The Huygens lander is released from the Cassini orbiter three weeks prior to the entry into Titan's atmosphere. Since the capsule does not have a control system, the state at the Entry Interface Point (EIP), 1270 km above Titan's surface, is subject to large uncertainties. After the lander decelerates aerodynamically, the first parachute is opened at an altitude of roughly 156 km [1, 3]. The flight phase from EIP to parachute deployment takes around 272 s and is investigated in this paper.

The nonlinear equations of motion are based on [17]. Given the limited space, we only outline the necessary assumptions and general approach. We refer the reader to [17] for an in depth discussion. First, the celestial body Titan is assumed to be spherical with a homogeneous mass distribution, such that its gravity can be described by a point mass. This is well suited for the atmospheric entry flight, since the aerodynamic forces and torques are the main driver of the system's dynamics. Titan also rotates with a constant angular velocity according to [18]. Furthermore, the capsule's heat shield ablation, which reduces the initial mass of 320 kg by roughly 10 kg during the entry flight, is neglected resulting in a constant mass of the capsule [3]. The products of inertia, which are less than 0.7 % of the diagonal elements (J_{xx}, J_{yy}, J_{zz}), are neglected as well. We neither consider wind in the equations of motion, since it would make the dynamics much more complex while having only a small impact on the flight due to the vehicle's high entry velocity. Last, Titan's recommended atmospheric model is taken from [19], whereas Huygens' aerodynamic database is given in [20]. A summary of Huygens' [3, 20] and Titan's [3, 18] properties are listed below.

Next, we choose the set of states, in which the equations of motion are expressed. During the entry flight, the vehicle covers a large range of the body's surface, such that Titan cannot be assumed as flat. It is also easier to interpret

*https://www.mosek.com

Property	Value
mass	$m = 320\,\mathrm{kg}$
moment of inertia	$J = diag(J_{xx}, J_{yy}, J_{zz}) = diag(127.75, 75.85, 71.9)\,\mathrm{kg\,m^2}$
center of mass	$x_{com} = \begin{bmatrix} -0.47176 & 0.00153 & 0.00493 \end{bmatrix}^T \mathrm{m}$
moment reference center	$x_{mrc} = \begin{bmatrix} -0.71383 & 0 & 0 \end{bmatrix}^T \mathrm{m}$
reference area	$A_{ref} = 5.73\,\mathrm{m^2}$
reference length	$L_{ref} = 2.7\,\mathrm{m}$

Table 1 Vehicle's properties

Property	Value
Gravitational constant	$\mu_T = 8.98\mathrm{e}12$
Mean radius	$R_T = 2575\,\mathrm{km}$
Angular velocity	$\Omega_T = 4.56\mathrm{e}{-6}\,\mathrm{s^{-1}}$

Table 2 Titan's properties

spherical coordinates in combination with a spherical body. For these reasons, the translational motion is described by spherical position and velocity states in the rotating frame of the central body. In addition, due to Titan's significant atmosphere, the translational and rotational motions of the entry flight are both strongly dominated by the aerodynamic forces and torques, thus, we use states relative to the aerodynamic reference frame. As wind is excluded from the analysis, the aerodynamic-based and flight-path-frame-based values are identical making it easy to obtain the former values. Consequently, we use the aerodynamic angles angle of attack α, sideslip angle β, and bank angle μ together with the body-fixed angular velocities p, q, and r for the rotational motion. The states are summarized hereafter.

Translational states	Symbol
Radius	R
Longitude	τ
Latitude	δ
Aerodynamic velocity	V_a
Aerodynamic flight path angle	γ_a
Aerodynamic heading	χ_a

Table 3 Translational states

Rotational states	Symbol
Angle of attack	α
Sideslip angle	β
Bank angle	μ
Roll rate	p
Pitch rate	q
Yaw rate	r

Table 4 Rotational states

With these assumptions and definitions, we obtain the analytical nonlinear equations of motion for Huygens' atmospheric entry flight. Since the derived dynamics represent a nonlinear uncontrolled system, they can be written down in the form of Eq. (1). Here, Huygens' and Titan's properties listed in the Tables 1 and 2 define the parameters p, whereas the states $\tilde{x}$ are given in the Tables 3 and 4. Furthermore, the nominal initial states of the nonlinear system $\tilde{x}(0)$ are specified in Table 5. By investigating the nominal trajectory, high frequency oscillations are identified in the rotational states α, β, q, and r. Therefore, Huygens' nonlinear equations of motion are linearized according to Subsection II.C with trimmed conditions for these states. Last, the uncertain initial states ξ of the resulting LTV model are defined in order to perform the robustness analysis. Although all initial states of the Huygens mission are subject to uncertainties [2, 3], only a deviation of the initial radius of maximum $\Delta R(0) = 30.73\,\mathrm{km}$ is considered to simplify the problem, which corresponds to the 1σ value of Huygens' altitude at Entry Interface Point [3].

State	Initial value
Radius	$R(0) = 3845\,\mathrm{km}$
Longitude	$\tau(0) = -185.43°$
Latitude	$\delta(0) = -8.61°$
Velocity	$V_a(0) = 6047.23\,\mathrm{m\,s^{-1}}$
Flight path angle	$\gamma_a(0) = -64.85°$
Heading	$\chi_a(0) = 259.96°$
Angle of attack	$\alpha(0) = -3.46°$
Sideslip angle	$\beta(0) = 3.41°$
Bank angle	$\mu(0) = -135.04°$
Roll rate	$p(0) = -44.4\,^\circ\,\mathrm{s^{-1}}$
Pitch rate	$q(0) = -2.06\,^\circ\,\mathrm{s^{-1}}$
Yaw rate	$r(0) = 2.39\,^\circ\,\mathrm{s^{-1}}$

Table 5 Initial state values

V. Results

The overall goal is to consider all initial states as uncertain and to include all the components of the higher order term as quadratic constraints to account for the linearization errors. However, we only take an uncertain initial radius and the higher order term component of the aerodynamic velocity's time derivative $\dot{V}_a$ into account here to show the general functionality of the developed robustness analysis. Using the whole set of uncertainties and nonlinearities will be considered in future research. Subsequently, the developed method is analyzed in two steps. First, only the effect of an uncertain initial radius is investigated by assuming the linearized model dynamics to be accurate over the whole state space; this refers to a nominal worst-case analysis. Thereafter, we extend the analysis by including the quadratic constraint of the aerodynamic velocity's time derivative. In both cases, the vector y is reduced to the single component y_l to obtain an individual upper bound on the final state.

For the nominal worst-case analysis, Theorem 1 simplifies significantly. The optimization problem contains only the free parameter v_1 and simplifies to

$$\dot{P} = -PA - A^T P \quad \forall t \in [0, T] \tag{21}$$

$$I_l^T I_l - P(T) = 0 \tag{22}$$

$$\begin{bmatrix} p_{11}(0) - v_1 & 0 \\ 0 & v_1 - \gamma^2 \end{bmatrix} \leq 0. \tag{23}$$

Here, p_{11} is the component in the first row and column of matrix P and I_l denotes the l-th row of the identity matrix. Figure 2 shows the upper bound results for the states radius (Fig. 2a), aerodynamic velocity (Fig. 2b), and flight path angle (Fig. 2c) over time. Since the theorem only determines γ at the time point T, the upper bound is calculated at 30 different T, which are equally spaced over the investigated flight phase, and is visualized by a dot marker. Additionally, the figures also show linear and nonlinear envelopes, abbreviated with "lin" and "nonlin", respectively. These curves are obtained by performing perturbed simulations with the linear and nonlinear model and taking the absolute maximum over the simulations. As shown in Fig. 2, the calculated upper bounds match the linear envelopes perfectly. This validates the core of the developed robustness analysis method, i.e. finding a valid and preferably optimal upper bound of the linear model. However, as expected, the calculated upper bounds are below the nonlinear envelopes in Fig. 2 demonstrating that these γ values are no valid bounds for Huygens' atmospheric entry flight. Therefore, higher order terms need to be considered in the analysis.

The second step of the analysis includes one quadratic constraint in addition to the uncertain initial radius. Therefore, the free parameters are v_1 and λ_1 and Eq. (11) has to be solved, whereas Eqs. (12) and (13) still simplify to Eqs. (12)

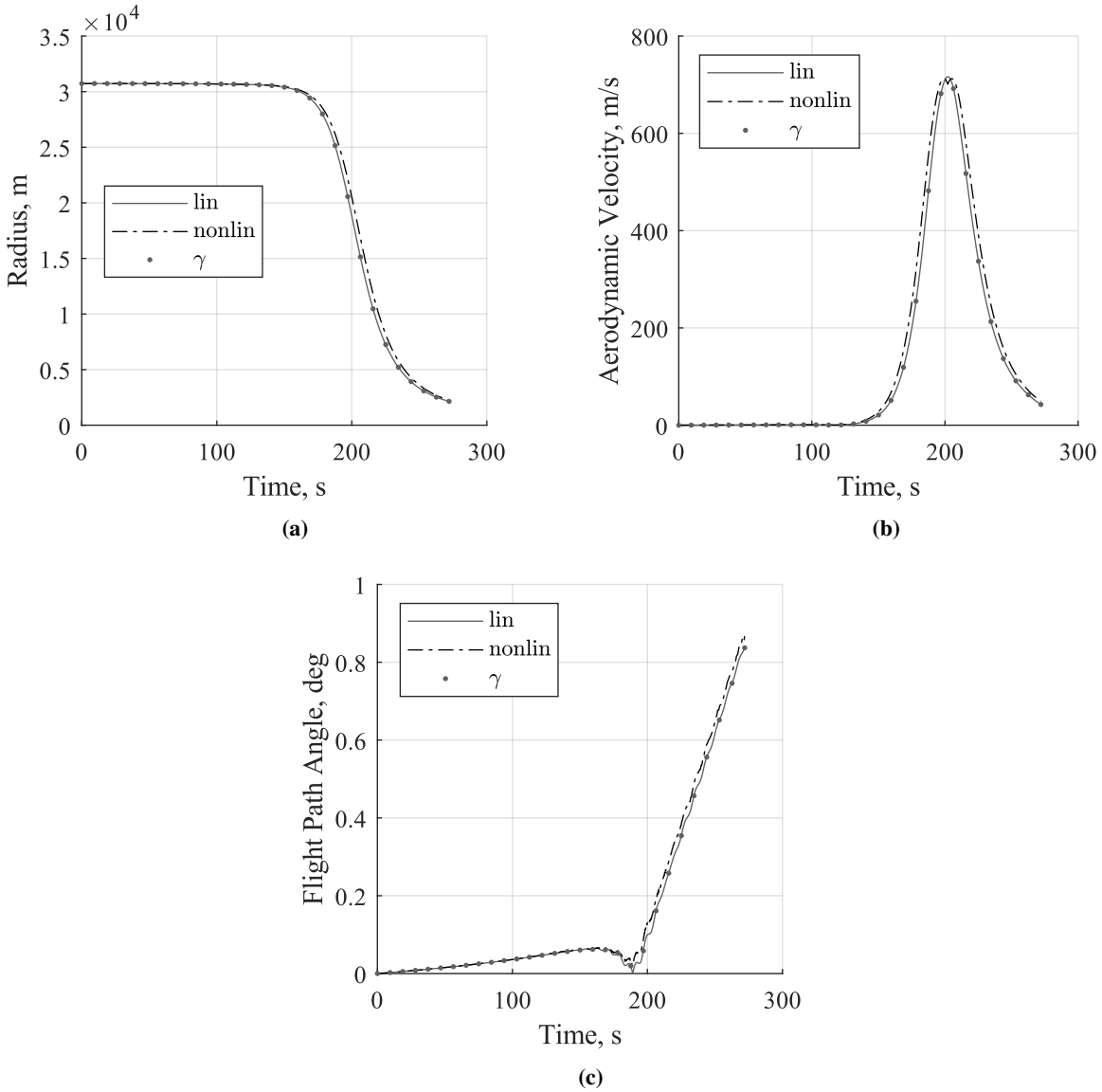

Fig. 2 Upper bound by simplified theorem for different states in comparison to linear and nonlinear envelopes. (a) Radius, (b) aerodynamic velocity, and (c) flight path angle.

and (23) due to a single uncertain initial state. In addition, the higher order term component of the aerodynamic velocity's time derivative is used as a quadratic constraint, since an uncertain initial radius mostly impacts the aerodynamic deceleration through the atmospheric density. As mentioned in Subsection II.D, a region around the nominal trajectory, expressed by upper bounds of the states, is necessary to determine the local quadratic constraint. Since finding the optimal constraint over many dimensions is computationally expensive and since the atmospheric density depends solely on the radius, the local quadratic constraint is calculated by using only the radius deviation from the nominal trajectory. However, the upper bound of the radius is unknown a priori. Therefore, the upper bound from the first step of the analysis, which is shown in Fig. 2a as γ, is used as an initial deviation. The robustness analysis as well as finding the optimal quadratic constraint are repeated iteratively until the upper bound result of the analysis is lower or equal to the γ values of the radius, that was used to determine the quadratic constraint. This is usually achieved after few iterations.

The robustness analysis results of the second step are shown in Fig. 3. These figures augment Fig. 2 by adding the upper bounds of three iterations that include the quadratic constraint. The additional upper bounds are denoted by $\gamma_{QC,n}$ with n indicating the iteration number. First, the $\gamma_{QC,1}$ values are located above or at the same level as the γ values at

every investigated time point. The same is true for each upper bound compared to its preceding iteration. This behavior matches the expectation, since adding a quadratic constraint to the analysis results in covering more dynamical variety, which itself leads to higher upper bounds. In addition, a quadratic constraint always contains its preceding constraint, since the previous region around the nominal trajectory is still included when the region is extended. Therefore, the upper bound also increases with each iteration. Next, the results $\gamma_{QC,2}$ and $\gamma_{QC,3}$ overlap, indicating that the iteration process has converged and the final solution with respect to the simplified analysis is found. As shown in Fig. 3, the upper bounds $\gamma_{QC,3}$ describe the shape of the nonlinear envelopes well, which demonstrates that Theorem 1 is set up and solved correctly. However, the γ values exceed the nonlinear envelope significantly at the end of the flight in Fig. 3a and around 200 s in Fig. 3b, indicating some conservatism.

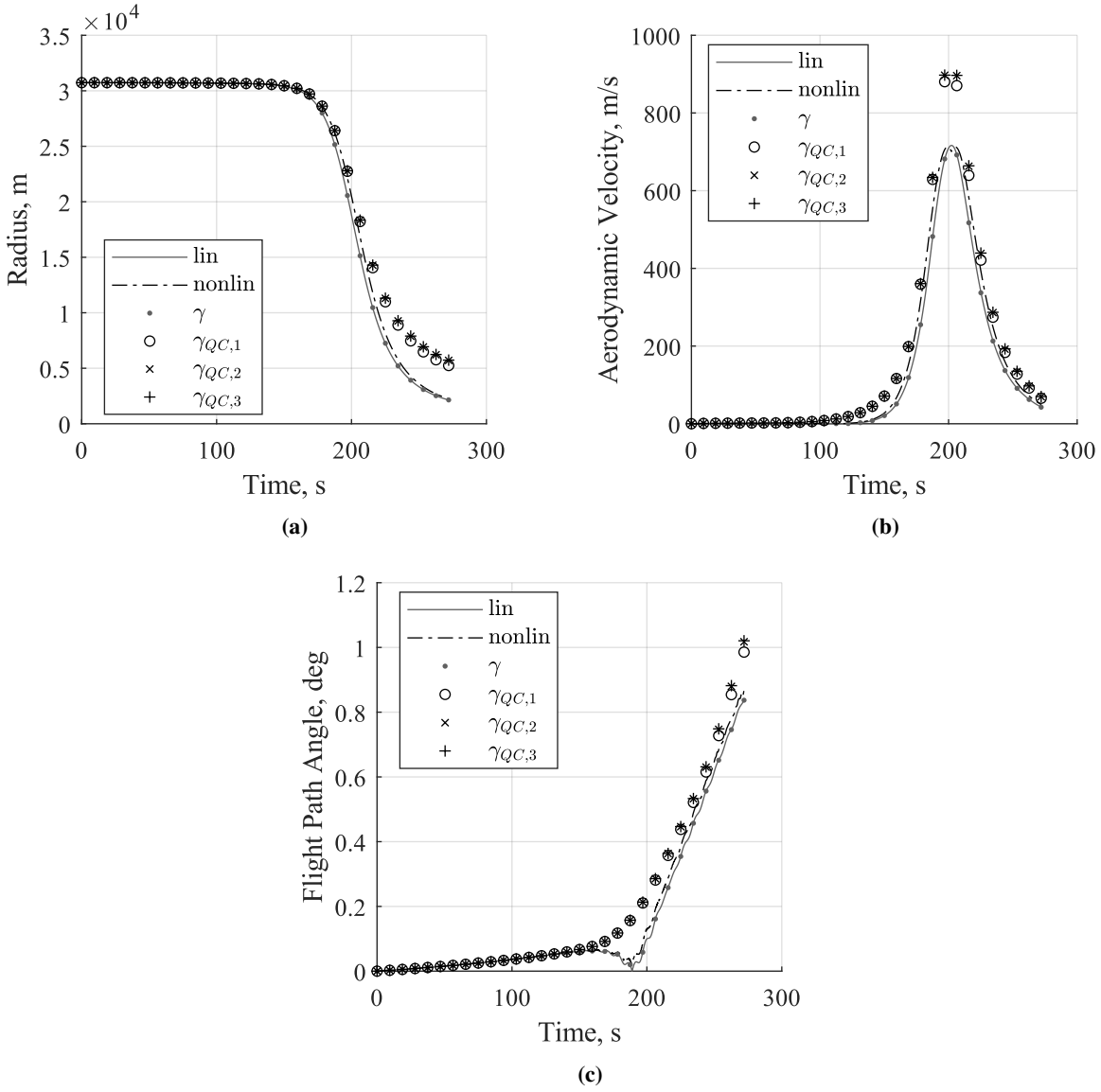

Fig. 3 Upper bound γ_{QC} by Theorem 1 and upper bound γ by simplified theorem for different states in comparison to linear and nonlinear envelopes. (a) Radius, (b) aerodynamic velocity, and (c) flight path angle.

VI. Conclusion

This paper presents a robustness analysis method for a nonlinear system under uncertain initial states. It is based on a linear time-varying model and local quadratic constraints that are optimized for the relevant region around the nominal trajectory. The individual steps to set up an LTV model and the local quadratic constraints for the analysis are outlined and the relevant theorem is derived. The method is applied to a simplified case of Huygens' atmospheric entry flight to show its proper functionality. The results show, that Theorem 1 is set up and solved correctly. Subsequent research will focus on obtaining less conservative results to improve the performance and extending the analysis to all uncertain initial states and quadratic constraints to obtain valid upper bounds for Huygens' entry flight. Overall, the proposed method has the potential to complement the flight dynamics analysis by providing upper bounds to system states and to accelerate the development process. Furthermore, there are ongoing missions similar to Huygens like NASA's Dragonfly mission [21], which is scheduled to launch in 2028 and will enter Titan's atmosphere in 2034, underlining the importance of efficient robustness analysis tools for systems influenced by uncertain initial conditions.

References

[1] Lebreton, J.-P., Witasse, O., Sollazzo, C., Blancquaert, T., Couzin, P., Schipper, A.-M., Jones, J. B., Matson, D. L., Gurvits, L. I., Atkinson, D. H., Kazeminejad, B., and Pérez-Ayúcar, M., "An overview of the descent and landing of the Huygens probe on Titan," *Nature*, Vol. 438, No. 7069, 2005, pp. 758–764. https://doi.org/10.1038/nature04347.

[2] Powell, R. W., Lockwood, M. K., Cruz, J. R., Striepe, S. A., Hollis, B. R., J., W. M., Justus, J., Duvall, A., Keller, V. W., Bose, D., Prabhu, D., Chen, Y. K., Olejniczak, J., Sutton, K., Fisher, J., and Takashima, N. T., "Cassini/Huygens Probe Entry, Descent, and Landing (EDL) at TitanIndependent Technical Assessment," Tech. rep., NASA Langley Research Center, 2009. URL https://ntrs.nasa.gov/api/citations/20090022173/downloads/20090022173.pdf.

[3] Kazeminejad, B., Atkinson, D. H., Pérez-Ayúcar, M., Lebreton, J.-P., and Sollazzo, C., "Huygens' entry and descent through Titan's atmosphere—Methodology and results of the trajectory reconstruction," *Planetary and Space Science*, Vol. 55, No. 13, 2007, pp. 1845–1876. https://doi.org/10.1016/j.pss.2007.04.013.

[4] Farhood, M., "Robustness analysis of uncertain time-varying systems with unknown initial conditions," *International Journal of Robust and Nonlinear Control*, Vol. 34, No. 4, 2023, pp. 2472–2495. https://doi.org/10.1002/rnc.7094.

[5] Biertümpfel, F., Theis, J., and Pfifer, H., "Robustness Analysis of Nonlinear Systems Along Uncertain Trajectories," *IFAC-PapersOnLine*, Vol. 56, No. 2, 2023, pp. 5831–5836. https://doi.org/10.1016/j.ifacol.2023.10.075.

[6] Seiler, P., and Venkataraman, R., "Trajectory-based robustness analysis for nonlinear systems," *International Journal of Robust and Nonlinear Control*, Vol. 34, No. 2, 2023, pp. 910–926. https://doi.org/10.1002/rnc.7009.

[7] Takarics, B., and Seiler, P., "Gain scheduling for nonlinear systems via integral quadratic constraints," *2015 American Control Conference (ACC)*, IEEE, 2015, pp. 811–816. https://doi.org/10.1109/acc.2015.7170834.

[8] Pfifer, H., and Seiler, P., "Robustness analysis of linear parameter varying systems using integral quadratic constraints," *2014 American Control Conference*, IEEE, 2014, pp. 4476–4481. https://doi.org/10.1109/acc.2014.6858751.

[9] Robens, J., and Pfifer, H., "Efficient Robustness Analysis along a Trajectory with Uncertain Initial Conditions," *IFAC-PapersOnLine*, 2026. Submitted for publication.

[10] Akima, H., "A method of bivariate interpolation and smooth surface fitting based on local procedures," *Communications of the ACM*, Vol. 17, No. 1, 1974, pp. 18–20. https://doi.org/10.1145/360767.360779.

[11] Pfifer, H., and Seiler, P., "An Overview of Integral Quadratic Constraints for Delayed Nonlinear and Parameter-Varying Systems," 2015. https://doi.org/10.48550/ARXIV.1504.02502.

[12] Megretski, A., and Rantzer, A., "System analysis via integral quadratic constraints," *IEEE Transactions on Automatic Control*, Vol. 42, No. 6, 1997, pp. 819–830. https://doi.org/10.1109/9.587335.

[13] Veenman, J., Scherer, C. W., and Köroğlu, H., "Robust stability and performance analysis based on integral quadratic constraints," *European Journal of Control*, Vol. 31, 2016, pp. 1–32. https://doi.org/10.1016/j.ejcon.2016.04.004.

[14] Skogestad, S., and Postlethwaite, I., *Multivariable feedback control*, 2nd ed., Wiley, Chichester, 2010.

[15] Biertümpfel, F., Pholdee, N., Bennani, S., and Pfifer, H., "Finite Horizon Worst Case Analysis of Linear Time-Varying Systems Applied to Launch Vehicle," *IEEE Transactions on Control Systems Technology*, Vol. 31, No. 6, 2023, pp. 2393–2404. https://doi.org/10.1109/tcst.2023.3260728.

[16] Lofberg, J., "YALMIP: a toolbox for modeling and optimization in MATLAB," *IEEE International Conference on Robotics and Automation (IEEE Cat. No.04CH37508)*, IEEE, 2004, pp. 284–289. https://doi.org/10.1109/cacsd.2004.1393890.

[17] Vinh, N. X., *Optimal trajectories in atmospheric flight*, No. 2 in Studies in astronautics, Elsevier, Amsterdam [u.a.], 1981.

[18] Archinal, B. A., Acton, C. H., A'Hearn, M. F., Conrad, A., Consolmagno, G. J., Duxbury, T., Hestroffer, D., Hilton, J. L., Kirk, R. L., Klioner, S. A., McCarthy, D., Meech, K., Oberst, J., Ping, J., Seidelmann, P. K., Tholen, D. J., Thomas, P. C., and Williams, I. P., "Report of the IAU Working Group on Cartographic Coordinates and Rotational Elements: 2015," *Celestial Mechanics and Dynamical Astronomy*, Vol. 130, No. 3, 2018. https://doi.org/10.1007/s10569-017-9805-5.

[19] Waite, J., Bell, J., Lorenz, R., Achterberg, R., and Flasar, F., "A model of variability in Titan's atmospheric structure," *Planetary and Space Science*, Vol. 86, 2013, pp. 45–56. https://doi.org/10.1016/j.pss.2013.05.018.

[20] Tran, P., and Lenoir, S., "Huygens Program - Entry Module Aerodynamic Database," Tech. rep., EADS Space Transportation, 2004.

[21] Lorenz, R., Turtle, E., Barnes, J., Trainer, M., Adams, D., Hibbard, K., Sheldon, C., Zacny, K., Peplowski, P., Lawrence, D., Ravine, M., McGee, T., Sotzen, K., MacKenzie, S., Langelaan, J., Schmitz, S., Wolfarth, L., and Bedini, P., "Dragonfly: A rotorcraft lander concept for scientific exploration at titan," *Johns Hopkins APL Technical Digest (Applied Physics Laboratory)*, Vol. 34, No. 3, 2018, pp. 374–387. Publisher Copyright: © John Hopkins University. All rights reserved.